J. Fluid Mech. (2003), *vol.* 490, *pp.* 75–98.
DOI: 10.1017/S0022112003005202 Printed in the United Kingdom

On the use of microjets to suppress turbulence in a Mach 0.9 axisymmetric jet

By V. H. ARAKERI†, A. KROTHAPALLI, V. SIDDAVARAM, M. B. ALKISLAR AND L. M. LOURENCO

Department of Mechanical Engineering, 2525 Pottsdamer Street, Florida A&M University and Florida State University, Tallahassee, FL-32310, USA

(Received 22 April 2002 and in revised form 19 March 2003)

We have experimentally studied the effect of microjets on the flow field of a Mach 0.9 round jet. Planar and three-dimensional velocity field measurements using particle image velocimetry show a significant reduction in the near-field turbulent intensities with the activation of microjets. The axial and normal turbulence intensities are reduced by about 15% and 20%, respectively, and an even larger effect is found on the peak values of the turbulent shear stress with a reduction of up to 40%. The required mass flow rate of the microjets was about 1% of the primary jet mass flux. It appears that the microjets influence the mean velocity profiles such that the peak normalized vorticity in the shear layer is significantly reduced, thus inducing an overall stabilizing effect. Therefore, we seem to have exploited the fact that an alteration in the instability characteristics of the initial shear-layer can influence the whole jet exhaust including its noise field. We have found a reduction of about 2 dB in the near-field overall sound pressure level in the lateral direction with the use of microjets. This observation is qualitatively consistent with the measured reduced turbulence intensities.

1. Introduction

Using various techniques, it has clearly been demonstrated that, for both subsonic and supersonic round jets, the dominant noise producing region is restricted to about two potential core lengths, or up to about $x/D = 20$ (e.g. Laufer, Schlinker & Kaplan 1976; Fisher, Harper-Bourne & Glegg 1977; Schaffer 1979; Norum & Siener 1982). This may be expected, since not only do the mean velocities remain high in this region, but also the turbulence intensities reach a peak (Bradshaw, Ferriss & Johnson 1964). The initial zone of a turbulent jet ($x/x_c \leqslant 2$, where x_c is the length of the potential core), is known to be dominated by organized large-scale (compared to the jet diameter) structures (e.g. Bradshaw *et al.* 1964; Crow & Champagne 1971; Yule 1978; and a review by Hussain 1983). The existence of these structures, which are described by different terminology such as eddies, vortices, coherent structures, instability waves, etc., has not only been inferred from flow-visualization studies, but also from hot-wire and near-field microphone measurements. They are found to exist in high-Reynolds-number jets, both with initially laminar and turbulent boundary

† On leave from Indian Institute of Science, Bangalore, India.

layers (Zaman & Hussain 1984), in high subsonic Mach number jets (Moore 1977) and in supersonic jets (Troutt & McLaughlin 1982; Lepicovsky *et al.* 1987). With selective forcing, acoustically for example, a semblance of control of these structures is possible and they become easily identifiable; whereas, in natural jets and, in particular, at higher Reynolds numbers, the detection is far more difficult and requires the use of conditional sampling techniques (Zaman & Hussain 1984). The connection between the large-scale structures and the far-field noise of a jet has been the subject of intense debate. In high-Mach-number jets, where the structure convection velocities can be supersonic, an effective noise source, termed as Mach wave radiation (Phillips 1960; Bishop, Ffowcs Williams & Smith 1971), is an example of a direct connection. Experimentally, optical methods have been used to detect and characterize these waves. In one set of extensive studies using shock tubes, Oertel (1979) has inferred the existence of three distinct convection Mach numbers which are in turn related to the jet Mach number, the jet temperature and the ambient temperature. A theoretical basis for the observed set of waves has been provided by Tam & Hu (1989). At relatively lower jet Mach numbers, where convection velocities are expected to be subsonic, it has not been possible to establish a direct connection between the large-scale structures and the far-field radiated noise field, but their role is thought to be important.

Near-field microphone measurements, for example by Mollo-Christensen (1967), have shown that pressure fluctuations arrive in rather well-defined wave packets suggesting that they are associated with the well-organized structures existing within the jet. Further, Bradshaw (1966) has indicated that an audibly perceptible decrease in the noise levels was observed when the boundary layer in the nozzle was tripped. However, more convincing evidence comes from studies involving the effects that a forced jet has on the resulting far-field noise characteristics. As an example, Moore (1977) has shown that acoustical forcing can increase not only the far-field noise levels, but also the turbulence intensities in the jet. This effect was found to persist at high Reynolds numbers (exceeding 0.5 million) and high subsonic Mach numbers. On the other hand, there are other studies (e.g. Kibens 1980), which show that, by selective forcing, broadband far-field noise levels can decrease at the expense of an increase in the amplitude of the tonal components. Crighton (1981) has reviewed these contradictory findings and is of the opinion that whether there is an increase or a decrease in the broadband far-field noise levels due to external excitation, there seems to be a primary dependence on whether the experiments were at a Reynolds number higher or lower than 0.5 million; with an increase generally occurring at higher Reynolds numbers. It should be noted that the response of a jet to acoustic excitation is selective and is related to an issue first addressed by Crow & Champagne (1971). From an experimental study, they found that a turbulent jet possesses a dominant jet column instability mode with the corresponding Strouhal number being about 0.3. Other investigators have found different values, but still close to about 0.5. Crow & Champagne discuss their observations in relation to the results from a linear instability analysis due to Batchelor & Gill (1962). They found that the observed modes obey the dispersion relation for the wave speed predicted by Batchelor & Gill, but there is nothing in the theory which points to a dominant instability mode which receives the maximum amplification. The analysis of Batchelor & Gill was limited to the top-hat velocity profile and a velocity profile which is more characteristic downstream of the potential core. The latter profile was found to be stable in regard to axisymmetric disturbances, but unstable to a helical mode; whereas, the top-hat profile was unstable to the axisymmetric mode with predicted increasing amplification

with an increase in the frequency, or the Strouhal number. This clearly suggested that the jet instability characteristics are dependent on the nature of the mean velocity profile. It was Michalke (1971) who showed that the dominant mode observed by Crow & Champagne can, in fact, be predicted based on parallel flow linear instability analysis, provided the measured mean turbulent velocity profiles are used. Therefore, the selection process of the dominant jet column instability mode is then associated with the changing mean velocity profiles as the jet develops. Now, many investigations on jet turbulence have shown that the large-scale structures are consequence of the instability of the turbulent shear layer, even though there are differing points of view on this interpretation (Hussain 1983). In addition, it is worth pointing out that there are several jet noise prediction schemes that are based on instability theory models (e.g. Tam & Burton 1984; Liu 1974; Chan 1977).

Providing the basic understanding of jet noise has been the motivation for many of the investigations on jet turbulence, including those of Bradshaw *et al*. (1964) and Crow & Champagne (1971). This topic is still of current interest even though the emphasis is now on generating jet noise predictive capabilities and also looking at methods to reduce noise. Some of the techniques (mostly passive) being currently investigated are: modification of the nozzle exit (McCormick & Bennett 1993), use of non-axisymmetric nozzle shapes (Alvi *et al.* 1996; Zaman 1999), use of tabs (Zaman 1994) and use of flexible elements (Anderson, Wygnaski & Gutmark 1999). These have shown varied promise, but there is definite scope for considering alternative techniques, in particular those which do not interfere with the primary nozzle and which may also be amenable to active control. One such technique is the use of microjets at the nozzle exit. Alvi *et al.* (2000) have found that the use of microjets can be very effective in eliminating screech and impingement tones from supersonic jets. These noise sources are excellent examples which involve many of the jet turbulence constituents discussed earlier, namely, the large-scale structures, the response of a jet to excitation and the instability modes. In the case of screech and impingement tones the excitation is self-driven through a feedback mechanism (e.g. Powell 1953; Krothapalli *et al.* 1999). The fact that the use of microjets was able to either eliminate or substantially reduce the tone intensities (Alvi *et al.* 2000) suggests that the microjets interfere with one or more of the three constituents mentioned above. An investigation on this is one of the primary motivations for the present study. It was clear to us that measurement of the noise field alone would not be sufficient to throw light on the mechanism for the effectiveness of the microjets in noise suppression. For this reason, detailed velocity field measurements using particle image velocimetry (PIV) have been undertaken. However, we restricted our present study to a high subsonic Mach number to avoid complications from shocks. Studies at these Mach numbers are of interest by themselves from noise considerations (Simonich *et al.* 2001).

Another motivation for the present study was to provide a set of measurements on the turbulence and mean flow characteristics of a high subsonic Mach number jet; such data for a Mach 0.9 jet is lacking, as noted by Freund (2001). The primary reason for the lack of availability of data is associated with the difficulties in the use of hot wire at high velocities (some data by working at reduced pressures are available, Stromberg, McLaughlin & Trautt 1980, but these are limited to low Reynolds numbers). Optical methods are more suitable, and Lau, Morris & Fisher (1979) have provided one of the few detailed velocity measurements for a Mach 0.9 jet. However, they do point out certain discrepancies between laser-Doppler velocimetry (LDV) and hot-wire measurements carried out at a lower Mach number. PIV is a technique which can provide planar and three-dimensional velocity field

data simultaneously and certainly has a great advantage over LDV. Therefore, it was considered of interest to not only compare present measurements with those of Lau *et al.* (1979), but to also supplement them.

2. Experimental methods

2.1. *Test facility and PIV instrumentation*

The experiments were conducted using the blow-down compressed air facility of the Fluid Mechanics Research Laboratory (FMRL) at the Florida State University. The air used is supplied from a central high-pressure source (maximum pressure, 160 bar and a storage capacity of about $10\,m^3$). The nominal Mach 0.9 jet used in this study can be run continuously for about 1 h. After leaving the storage tanks, the air can be electrically heated when required. The air then passed through pressure regulators and control valves before entering a cylindrical plenum chamber. This is the point where the stagnation pressure and the stagnation temperature were monitored. Subsequently, the air entered a smaller cylindrical plenum. This chamber was approximately 100 cm long and had a circular cross-section of 5.92 cm in diameter; it housed a honeycomb and several screens placed in series. The flow finally emerged through a stainless steel nozzle ending with a diameter of 2.22 cm. At the end of the nozzle, the flow attained a 'top-hat' velocity profile with the exception of a thin boundary layer present near the solid surface. Under normal operating conditions, the boundary layer was nominally laminar. This could be confirmed from observation of small-scale instability waves, which were clearly visible in the single-shot PIV realizations. These waves, which have been termed as 'ripples' by Crow & Champagne (1971), could be removed by using a trip (1 mm in height and 4 mm in width) placed in the nozzle and thus making the boundary layer nominally turbulent under the tripped conditions. Unless otherwise specifically mentioned, the results pertain to a nominally laminar boundary layer at the exit.

The present tests were conducted with a stagnation pressure, P_0, of 10.8 p.s.i.g. ($\sim$1.73 bar) and a stagnation temperature, T_0, of 135°F ($\sim$330 K). The slight heating of the jet was used to avoid condensation. With these stagnation conditions, the resulting measured exit jet velocity, U_j, was about $315\,m\,s^{-1}$ and the corresponding nominal jet Mach number was 0.9. The jet Reynolds number, Re_D, based on U_j and the exit diameter is 0.5×10^6. The velocity and other measurements were made only when the P_0 value was within 1% of the above value.

Non-intrusive measurement of the velocity field was made using PIV. In most cases, the velocities were measured in a planar configuration and, when required, a stereoscopic PIV was used to obtain the three-dimensional velocity field data. Some details of the PIV technique and associated hardware used in the present experiments are available in Krothapalli *et al.* (1999) and a detailed discussion of the application of the stereoscopic PIV is provided in Alkislar (2001). Briefly, the PIV hardware consisted of a frequency doubled Nd-Yag laser with a dual cavity (Spectra-Physics PIV-400) for flow field illumination, a CCD camera with a resolution of $1008(H) \times 1018(V)$ pixels of a size of $9 \times 9\,\mu m^2$ for recording the images and a computer, with Pentium III CPU, to control the camera and acquire 256 image pairs at the maximum camera framing rate. In the present experiments, 15 image pairs per second were acquired with the time between two successive images in a pair being fixed at 1–2 μs. For planar velocity field measurements, a single camera was positioned at 90° to the jet axis and the optical arrangement was such that the image area covered was 12 cm × 12 cm. For PIV measurements, the jet was seeded with small ($\sim$0.1–1 μm) oil droplets generated

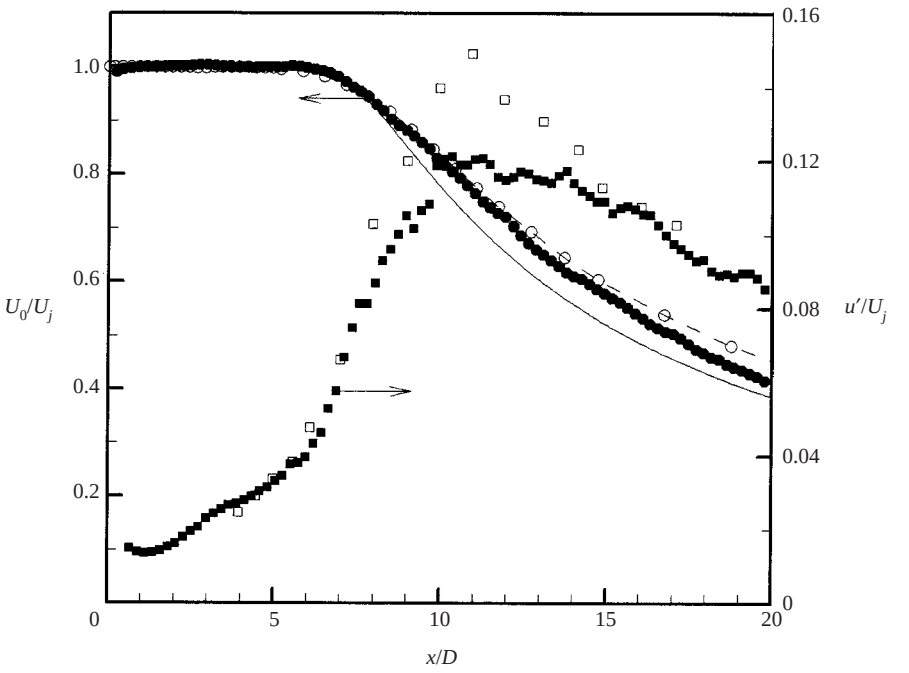

FIGURE 1. Centreline distribution of mean velocity, U_0/U_j: ●, present results; ——, Lau *et al.*; – –○– –, Simonich *et al.* and axial turbulence intensity, u'/U_j: ■, present results; □, Lau *et al.*

using a modified Write nebulizer and the ambient air was seeded with smoke particles (∼5 μm) produced by a Rosco fog generator. An image-matching approach was used for the digital processing of the image pairs to produce the displacement field. To achieve velocity data with high spatial resolution, a novel-processing algorithm developed by Lourenco & Krothapalli (1998) was used. The displacement between the image pairs was found by means of cross-correlation, and a velocity (displacement) vector is assigned to a second-order approximation. Thus, the velocity field at any point is described by a second-order polynomial analytical function using a least-squares-fitting algorithm. The marked advantage of this approach is that the velocity field is described at any point with second-order accuracy and thus computation of derivatives is accomplished with a higher precision. Mean and turbulent velocity fields were computed by processing 1000 image pairs, thus giving an accuracy of better than 1% in mean velocity measurements and better than 5% in turbulence intensity measurements.

To provide a measure of the accuracies attainable, one set of PIV results is compared with the LDV measurements of Lau *et al.* (1979) and recent Pitot measurements of Simonich *et al.* (2001) in figure 1. The centreline mean velocity and turbulence intensity covering the region from the nozzle exit to 20 diameters are included in the figure. The solid line in the figure corresponds to the expression provided by Lau *et al.* (1979) for the centreline velocity decay. The discrepancy between the present data and the line is due to the different potential core length observed in the present experiment. Our data indicate the potential core length to be about $6D$ as opposed to $5.2D$ as measured by Lau *et al.* (1979). The data of Simonich *et al.* (2001), included here as the dotted line in the figure, suggest that the length of the potential core is $6D$ and this observation is also supported by the results of Stromberg *et al.* (1980). The derived

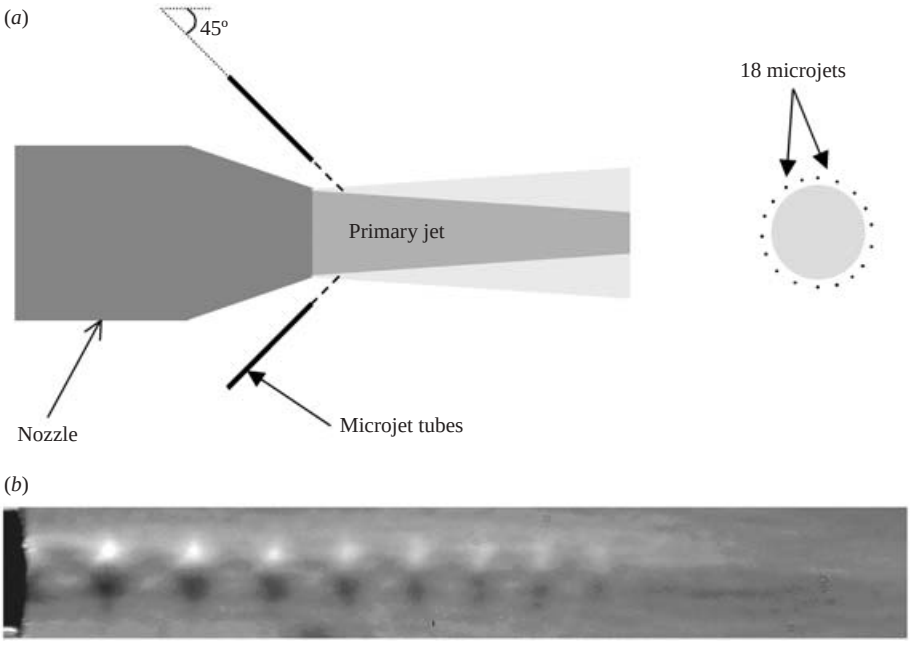

FIGURE 2. (*a*) The placement of the microjets with respect to the primary nozzle. (*b*) Schlieren flow visualization photograph of supersonic flow exiting from a 400 μm diameter tube. The fully expanded Mach number is about 1.4.

velocity from the pitot data of Simonich *et al.* (2001) is expected to have errors due to relatively high turbulence intensities far downstream of the jet, resulting in small discrepancies as shown in the figure. From these observations, it is suggested that the centreline velocity decay obtained from PIV measurements will have the least error in representing its behaviour. Also shown in the figure is the centreline variation of the turbulent velocity fluctuation, u' (here, u' represents the r.m.s. value), and similar data of Lau *et al.* (1979) is included for comparison. The general agreement is satisfactory; however, the peak value obtained by LDV is about 20% higher than the PIV data. The unusually higher peak values observed in the LDV measurements have been addressed at some length by Lau *et al.* (1979). The turbulence intensities measured using PIV are in accord with those in the literature obtained using hot wires (e.g. figure 5 in Moore 1977) and having established this consistency, the description of the microjets used to affect the primary jet exhaust is provided next.

2.2. *Microjets*

Eighteen microjets generated from a high-pressure source and exiting from 400 μm diameter tubes entered the primary jet at an angle of 45° to the nozzle axis (figure 2*a*). Air or nitrogen from a high-pressure gas cylinder was led to a cylindrical manifold through a pressure regulator, from which it was distributed to the 400 μm stainless steel tubes for creating the microjets. A precision mass flow meter was used to monitor the combined microjet discharge. In the present experiments, a combined mass flow rate of 90 SLPM (standard litre per minute) was used; this value corresponds to 1.12% of the primary jet mass flux. This microjet mass flow rate was possible by maintaining source stagnation conditions of $P_{0mj} = 5$ bar and $T_{0mj} = 300$ K; however, owing to pressure drop, the effective stagnation conditions were $P_{0mj} = 3.5$ bar and

$T_{0mj} = 300\,\mathrm{K}$. With these conditions, the microjet tube exit flow was choked and the fully expanded Mach number was supersonic having a value of about 1.4. Figure 2(*b*) is a schlieren flow-visualization photograph of an isolated microjet created under similar conditions to those used at present. The figure clearly shows the expected series of shock cell structures. Initially, the individual microjets are expected to penetrate and behave like a jet in cross-flow; but, subsequently, the combined influence of the microjets will be a global one. Capturing this effect was one of the objectives of the PIV measurements. The configuration and the operational conditions for the microjets chosen were similar to those used by Alvi *et al.* (2000).

2.3. *Near-field noise*

Limited near-field noise measurements were carried out using two B&K1/4-inch microphones (model 4136). These were placed in a line at a distance of 50 cm and such as to receive noise at angles of 90° and 30° to the jet axis. The microphone outputs were connected to a set of standard B&K amplifiers (model 2690A) and the data were recorded using a high-speed data-acquisition system. The post-processing involved the computation of the over-all sound pressure levels (OASPL) and narrowband spectra using a fast Fourier transform. It should be pointed out that the noise measurements were carried out with the microphone protective grid on. However, the computed spectra were corrected for the microphone grid effect by applying free-field corrections using the charts provided by B&K. The corrections are sensitively dependent on the direction of sound incidence; we used the corrections as applicable to random incidence. This method of applying free-field correction was verified by conducting tests in a separate test rig; in fact, the difference in the spectra obtained with and without the use of a microphone protective grid was nearly identical to the random incidence correction provided in the B&K chart.

Most of the objects in the vicinity of the microphones were covered with 5 cm sound absorbing material; however, the measurements cannot be considered anechoic. Since our interest was to look for differences in the jet noise characteristics with and without the use of the microjets, the procedure that we adopted for the noise measurements was considered adequate.

3. Results and discussion

3.1. *Effect of microjets on the flow field*

3.1.1. *Laminar exit boundary layer*

Using PIV, it was possible to map out the flow field at each point and hence, global information on the evolution of the jet could be obtained. In figures 3–6, we present the planar mean and turbulence characteristics of the jet in terms of contour plots. From the results presented in figures 4–6, the striking effect of the microjets in reducing the turbulence intensities is clearly brought out. The reductions seem to be across the entire shear layer, but are limited to an axial distance of about 12 diameters. It is significant to point out here that the observed turbulence suppression has been possible with a microjet mass flow rate of only about 1% of that of the primary jet. There are more subtle changes in the mean flow characteristics; these can be inferred from a closer examination of the results presented in figure 3. The potential core length is increased from a value of x_c/D of 6 to x_c/D of 7.5 (obtained from the centreline velocity distribution, similar to what is shown in figure 1) and thus the jet seems to have been stretched, an effect similar to that observed with a

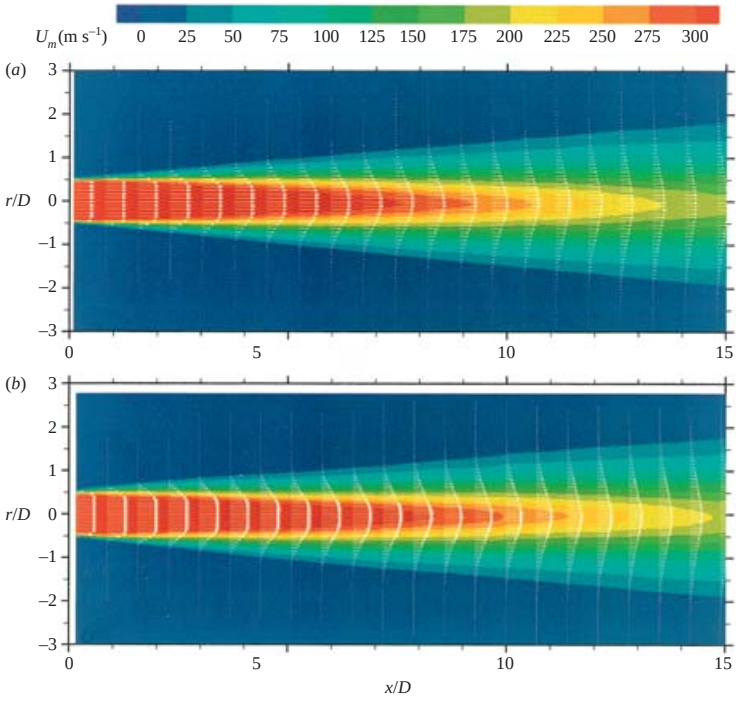

FIGURE 3. Mean velocity distribution in the central plane. (*a*) Normal jet; (*b*) with microjets.

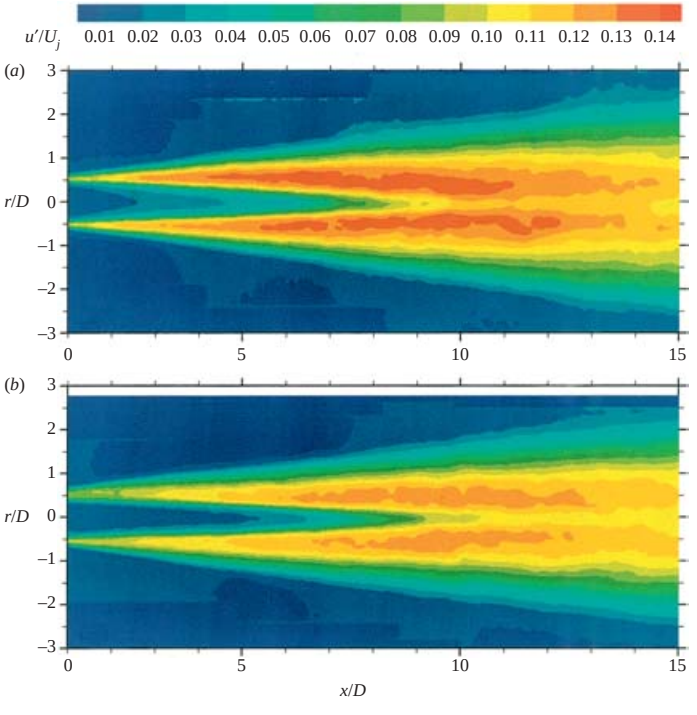

FIGURE 4. Axial turbulence intensity, u'/U_j distribution in the central plane. (*a*) Normal jet; (*b*) with microjets.

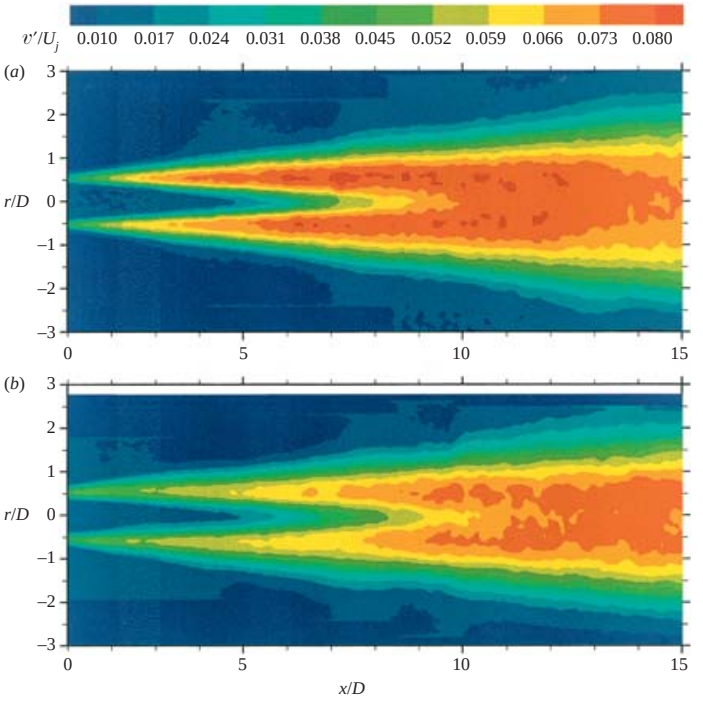

FIGURE 5. Transverse turbulence intensity, v'/U_j distribution in the central plane. (*a*) Normal jet; (*b*) with microjets.

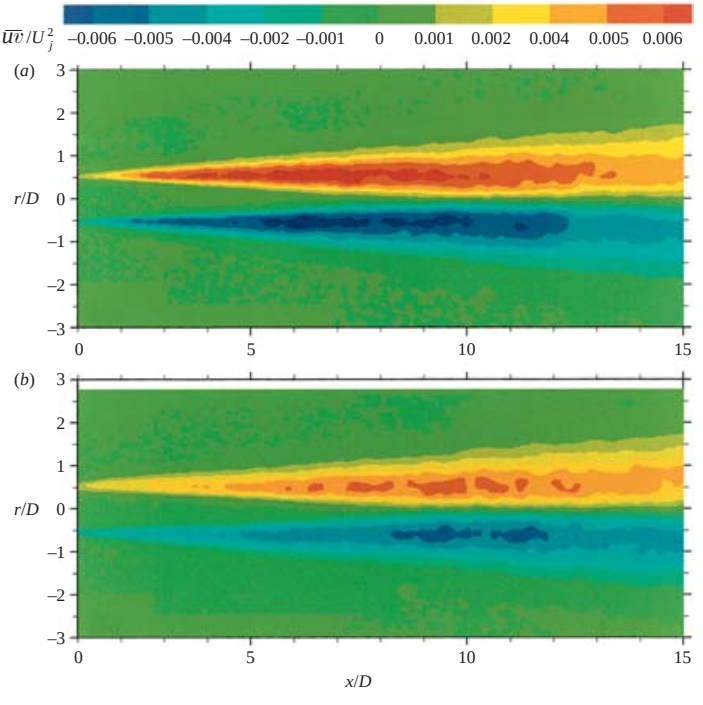

FIGURE 6. Turbulent shear stress, $\overline{uv}/U_j^2$ distribution in the central plane. (*a*) Normal jet; (*b*) with microjets.

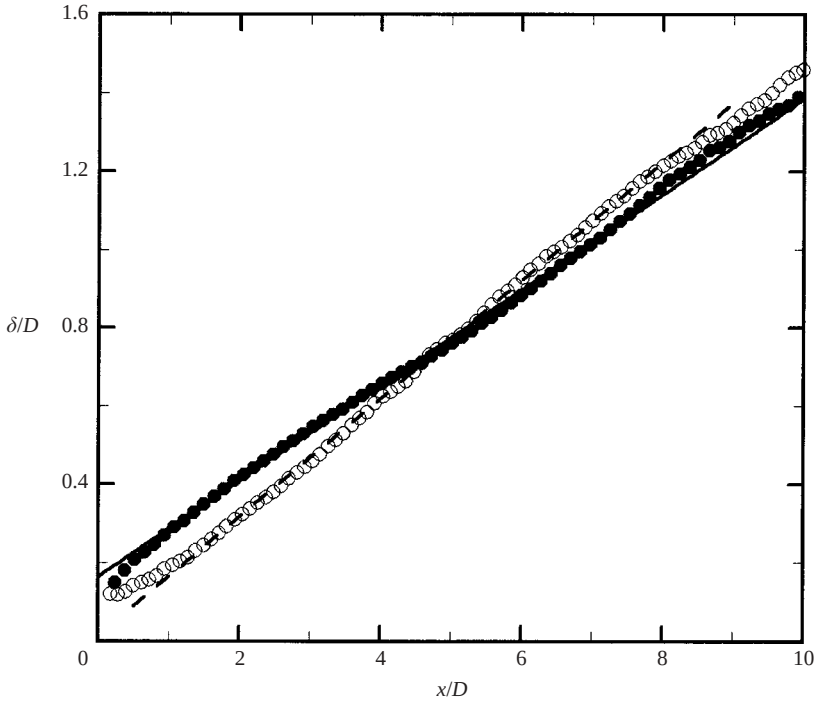

FIGURE 7. Streamwise variation of shear-layer width. ○, laminar – normal jet (slope of the linear fit = 0.133); ●, laminar – with microjets (slope of the linear fit = 0.105).

co-flow (Morris 1976). Consistent with this observation is the fact that the growth rate of the shear-layer width, defined as $\delta = (R_{0.95} - R_{0.10})$, with $R_{0.95}$ and $R_{0.10}$ being the radial locations at $U/U_0 = 0.95$ and 0.1, respectively, is reduced considerably in the initial region (figure 7). If the linear portions are extended, estimates for the location of the virtual origin can be obtained; for the normal jet, it is $x_0/D = -0.22$ and with microjets, it is shifted significantly upstream to $x_0/D = -1.6$. These values will be used later to examine the congruence of the mean velocity profiles using standard non-dimensional form (Hussain & Zedan 1978).

Figure 8 shows a quantitative measure of the extent of turbulent intensity reductions due to the use of microjets. Here, we show the variation of the peak values of u'/U_j, v'/U_j and $\overline{uv}/U_j^2$ (here the overbar denotes mean value) with axial distance up to about two potential core lengths and, as pointed out in § 1, this region being of importance from the noise point of view. The maximum reductions are found in the peak values of $\overline{uv}/U_j^2$, being up to about 40% at $x/D = 5$. We have examined and found that the correlation coefficient, R_{12}, defined as $\overline{uv}/u'v'$, is not significantly different in the two cases and hence, we conclude that the reductions in the covariance are as a result of reductions in the magnitudes of u' and v'. In figure 8, we also compare the peak values measured by Lau *et al.* (1979) using LDV. The general agreement cannot be considered good, even though it does improve at downstream locations. Our measurements are more consistent with recent hot-wire data due to Narayanan, Barber & Polak (2002) in a Mach 0.6 axisymmetric jet and therefore, could be taken to be more accurate.

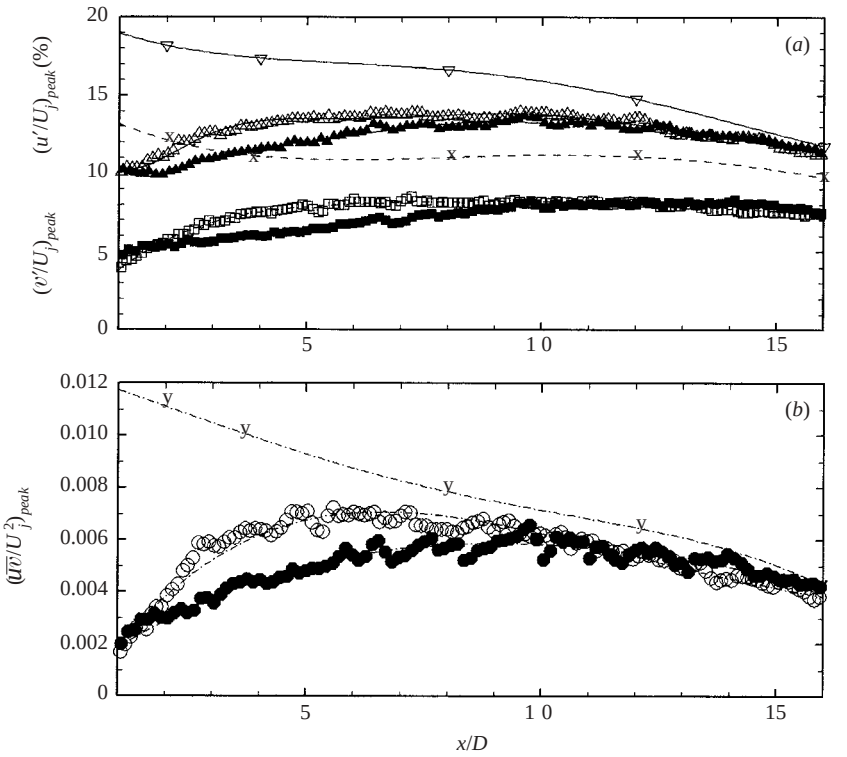

FIGURE 8. Streamwise variation of the peak turbulent parameters. (*a*) $(u'/U_j)_{peak}$: present results, △, normal; ▲, with microjets; ▽, data from Lau *et al.* $(v'/U_j)_{peak}$: present results, □, normal; ■, with microjets; X, data from Lau *et al.* (*b*) $(\overline{uv}/U_j^2)_{peak}$: present results, ○, normal; ●, with microjets; Y, data from Lau *et al.*

Close examination of the results presented in figure 8, shows that the measured Reynolds stress values in the near-field of the jet are quite low, being in the range of 0.003–0.006, in comparison to the expected values for a fully developed turbulent shear layer. For example, measurements due to Bradshaw *et al.* (1964) at $x/D = 2$ show a peak value of about 0.01. We suspect that in the present case, with the Mach number being high subsonic, the shear layer is not fully developed until much further downstream. This could also explain the fact that relatively low values of Reynolds stress are able to support a fairly substantial growth rate. In this context, it is of interest to compare our measurements with those of Narayanan *et al.* (2002); for example, at $x/D = 1$ the measurements reported in figure 16 of Narayanan *et al.* show peak values for u'/U_j and v'/U_j of about 0.06 and 0.05, respectively. If we assume a reasonable value of about 0.6 for the correlation coefficient R_{12}, then the estimate for $\overline{uv}/U_j^2$ is about 0.002, which is even less than what we have measured at $x/D = 1$. Therefore, our measurements seem to be fully consistent with measurements in the initial region of a high subsonic jet.

It is customary to examine the radial mean velocity profiles at successive downstream locations using non-dimensional similarity variables. A congruence of these is then an indication that the shear layer is approaching a self-preserving state. From such a plot, it is also possible to obtain an alternative measure of the spread

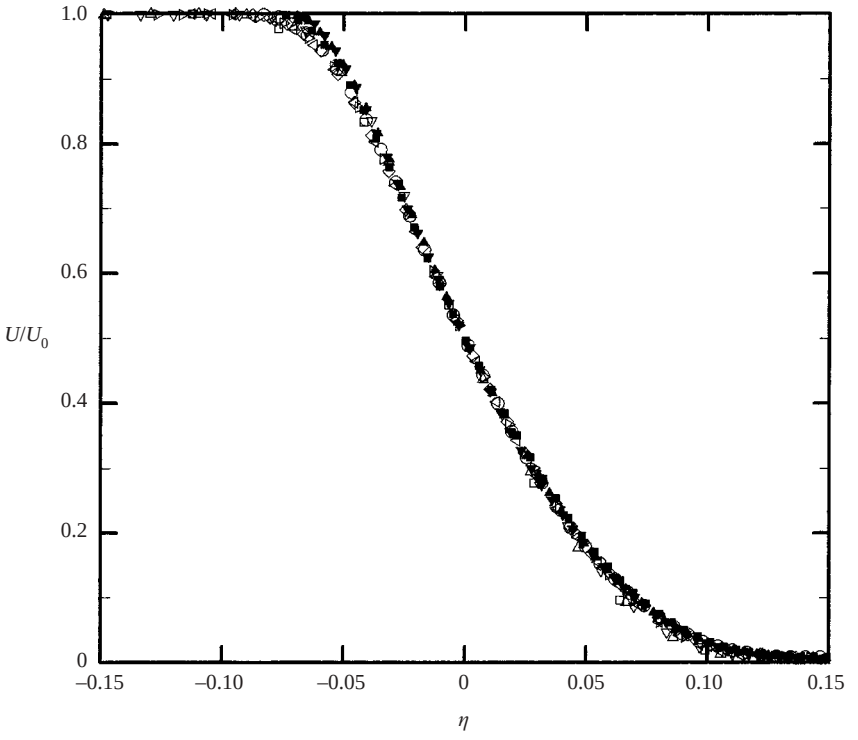

FIGURE 9. Mean velocity profiles from axial locations $x/D = 1$ to $x/D = 10$ in non-dimensional form for the normal jet. □, $x/D = 1$; △, $x/D = 2$; ∇, $x/D = 3$; ▷, $x/D = 4$; ◁, $x/D = 5$; ◇, $x/D = 6$; ○, $x/D = 7$; ■, $x/D = 8$; ▲, $x/D = 9$; ▼, $x/D = 10$.

rate, termed as vorticity growth rate, and denoted by δ_η(see figure 21 of Lau *et al.* 1979). A plot of the mean velocity data from $x/D = 1$ to $x/D = 10$, in the form U/U_0 versus $\eta = (r - R_{1/2})/(x - x_0)$, is shown in figures 9 and 10 for the cases of with and without the use of microjets. Here, $R_{1/2}$ is the radius at which $U/U_0 = 0.5$. The magnitudes of x_0, as indicated previously, were obtained from a plot of δ versus x/D (estimates based on using other thicknesses, like momentum and vorticity variation, were similar). Overall, a good collapse of the data is observed; it should be pointed out that without the use of x_0 in the definition of η (which is often followed) the collapse of the data would not be satisfactory at all. In figure 11, we show the variation of δ_η versus the jet Mach number, M_j, taken from Lau *et al.* (1979) as a solid line; also shown are present data obtained using figures 9 and 10. There is good agreement between the present estimate for the normal jet and the value obtained by Lau *et al.* at $M_j = 0.9$; however, with microjets the value is significantly lower and this is consistent with the observed reduced growth rate based on the variation of δ (figure 7). Therefore, from the results presented so far, we see that the effects of the microjets are to reduce the near-field turbulence intensities and the growth, or the spreading rate, of the jet. We have examined the influence of the microjets on some other parameters. A plot of the ratio of the local mass flux, $\dot{m}$, to the mass flux at the exit, $\dot{m}_e$ versus x/D can be used to estimate the entrainment. For the normal jet, the slope, $\mathrm{d}(\dot{m}/\dot{m}_e)/\mathrm{d}(x/D)$, was observed to vary from a value of 0.13 near the exit to a value of 0.24 further downstream; these values are in good agreement with those reported

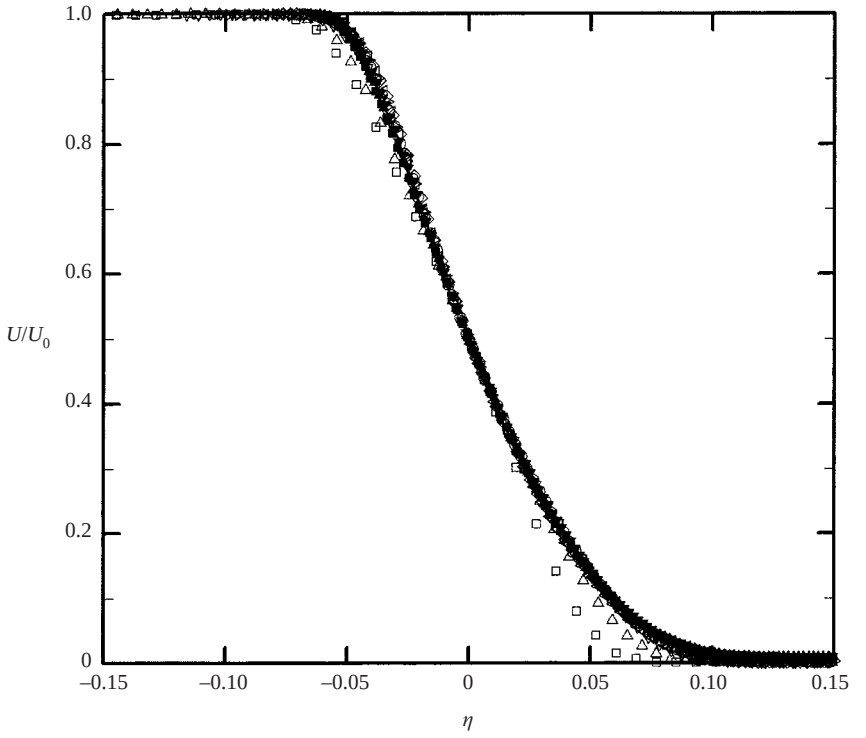

FIGURE 10. Mean velocity profiles from axial locations $x/D=1$ to $x/D=10$ in non-dimensional form for the case with microjets. □, $x/D=1$; Δ, $x/D=2$; ∇, $x/D=3$; ▷, $x/D=4$; ◁, $x/D=5$; ◇, $x/D=6$; ○, $x/D=7$; ■, $x/D=8$; ▲, $x/D=9$; ▼, $x/D=10$.

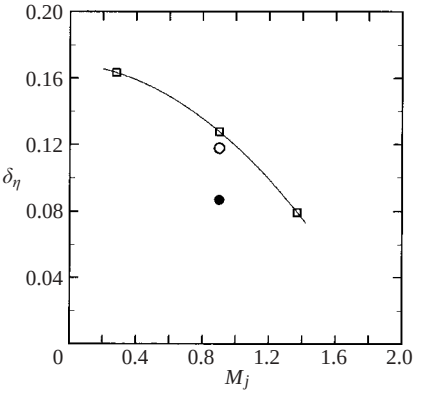

FIGURE 11. Variation of vorticity thickness growth rate, δ_η versus jet Mach number, M_j taken from Lau *et al.* (solid line). Present results: ○, normal; ●, with microjets.

by Crow & Champagne (1971) for a jet with a much lower Mach number and also with more recent measurements at a comparable Mach number due to Zaman (1999). With microjets, there were no significant differences in the slopes. Similarly, only a marginal effect was found on other quantities like the turbulence length scales, two-point velocity correlations and probability density function of axial turbulent velocity

fluctuation. As an example, the variation of the two-point correlation, R_{uu}, defined as

$$R_{uu} = \frac{\overline{u(x_0, r_0, t)u(x, r, t)}}{\overline{u(x_0, r_0, t)u(x_0, r_0, t)}},$$

is shown as a contour plot in figure 12, corresponding to a location of $x_0/D = 3$ and $r_0/D = 0.5$. Even though some differences appear to be present, they are not significant.

3.1.2. *Turbulent exit boundary layer*

A first impression of the role of the microjets would be that they simply act as a form of aerodynamic tripping device. If microjets are to be successful in suppressing turbulence, and hence noise, in a practical environment, they should prove to be effective under turbulent exit boundary-layer conditions as well. Therefore, we repeated the tests described earlier with a boundary-layer trip. Our finding is that the microjets not only serve as a form of tripping device, but also do something more. This becomes apparent from the observed quantitative differences as compared to the laminar case and we will present some results to highlight these. The shear-layer growth rate $\mathrm{d}\delta/\mathrm{d}x$, was found to decrease from a value of 0.128 to a value of 0.116; this change is smaller than that for the laminar case (figure 7). The variation of the peak value of the covariance, $\overline{uv}/U_j^2$, with axial distance for the turbulent cases tested is shown in figure 13. With microjets, there is reduction in the tripped case as was observed for the laminar case (figure 8); however, since there is some decrease in the peak values due to tripping itself, the effectiveness of the microjets under these conditions appears to be less. From our general observations with the use of microjets in the normal and tripped cases, it appears that an added effect of the microjets is to make the jet development less dependent on the initial conditions. For brevity, we do not present any additional results under tripped conditions here; however, they are available in Siddavaram (2002).

3.2. *Three-dimensional issues*

It is well known from several studies (e.g. Jiminez 1983; Bernal & Roshko 1986) that even though the dominant structures in a plane shear-layer are two-dimensional, three-dimensional features begin to appear at a rather early stage. For a round jet, Liepmann & Gharib (1992) have investigated these aspects in some detail. In the present study with microjets, the issue of three-dimensional effects assumes some significance, since the microjets entered the primary jet with regular azimuthal spacing. Our primary concern was whether the findings from the planar PIV studies (discussed above) reflect the happenings in the entire jet. For this reason, stereoscopic PIV studies at selected downstream locations were carried out. We present sufficient results here to illustrate the fact that the mean flow field was axisymmetric and that the observed turbulence reductions due to microjets were across the entire cross-section of the jet. The axial component of the mean velocity across a plane perpendicular to the jet axis, at a location of $x/D = 4$ is shown in figure 14. It is clear from the contour plots presented, that there are no observable three-dimensional effects due to the microjets. Even close to the nozzle exit, we could not pick up the imprints of the microjets, which suggests that they rapidly mix with the primary jet. However, it should be pointed out that the effects of microjets were seen as kinks in the computed azimuthal vorticity distribution and an illustration of this will be presented later. In figure 15, we

show the effect of microjets on the total turbulent kinetic energy, $TKE = q^2 = (u'^2 + v'^2 + w'^2)/2$, in the cross-plane at $x/D = 4$. The upper half shows the distribution of TKE under normal conditions (only the top portion is included since the results were similar in the lower portion) and the lower half shows the effects of the microjets. It is evident that there is an appreciable reduction in the TKE across the entire cross-sectional plane. From these results, and others not included (details can be found in Siddavaram 2002), we were convinced that the effects of microjets in turbulence suppression are not limited to the central plane in which the planar PIV studies were made, but occur within the entire jet cross-section up to x/D of about 10. What remains to be understood is the possible physical mechanism involved and we take up this issue in a subsequent section after presenting some results on the effect of the microjets on the noise field.

3.3. *Near-field noise*

As indicated previously, noise measurements in the near field were carried out at two angles from the jet axis, namely, 90° and 30°, and these were also done with the exit boundary layer being laminar as well as turbulent. However, the effect of the microjets on the near-field noise levels was found to be similar at both the angular locations and under normal and tripped conditions. Hence, in figure 16 we provide only one set of results, being representative of the effect of microjets on radiated noise. The spectra shown indicate a modest reduction, about 2 dB, in the near-field noise levels, primarily in the frequency range of about 5 to 25 kHz associated with the use of microjets; the corresponding decrease in OASPL was also of a similar magnitude. The spectra shown in figure 16 indicate a peak at about 3.5 kHz, and this corresponds to a Strouhal number of about 0.25. This is in agreement with other findings (e.g. Simonich *et al.* 2001); however, the general shape of the spectra is not. Even though the spectra at 90° are normally flatter than those at peak noise radiation angle of 30°, ours seem to be flat over a much wider high-frequency range. We suspect that the reason for this is primarily associated with the fact that the present measurements were in a non-anechoic environment. However, in spite of these differences from standard spectra, we believe the quoted reductions of about 2 dB can be taken as accurate representation of the possible levels of jet noise reduction due to the use of microjets. As shown in figure 16, this is the case with the exit boundary layer being laminar or turbulent. It is of interest to note from the same figure, that the tripping itself reduces the peak noise level by about 1 dB. The general noise reductions observed are comparable to those found with the use of tabs (Simonich *et al.* 2001).

4. Further discussion: the possible role of microjets

What we have observed is a large effect (turbulent shear stress reduction up to 40%) from a small cause (only about 1% mass flow rate in the microjets). Therefore, the microjets must play a role in influencing the most sensitive aspect of the jet flow dynamics. From existing knowledge, as reviewed in § 1, it appears logical to explain our findings based on jet stability considerations. We are further encouraged to follow this line of reasoning from the experience of Moore (1977), who found that both jet turbulence and noise are affected by small-amplitude acoustic excitation. In addition, in what can be considered a significant advance, Morris, Giridharan & Lilley (1990) and Viswanathan & Morris (1992) have been able to compute the turbulent shear-layer growth rate for the plane and axisymmetric cases without any empirical input, except for the form of the mean velocity profiles. In their model, the treatment of

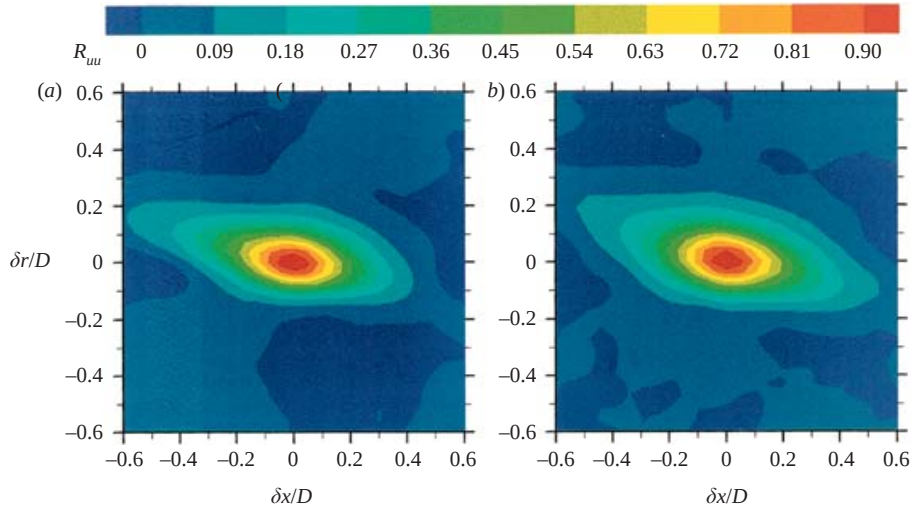

FIGURE 12. Distribution of two-point correlation of the axial turbulent intensity at $x_0/D = 3$ and $r_0/D = 0.5$.

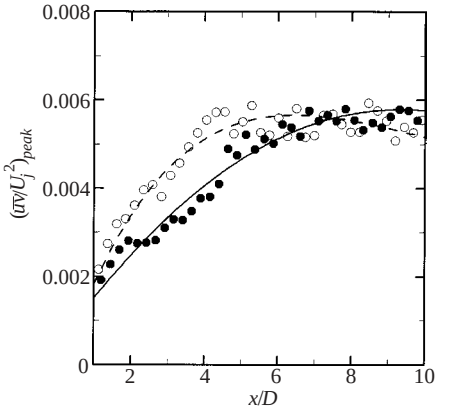

FIGURE 13. Streamwise variation of the peak covariance, $\overline{uv}/U_j^2$. ○, turbulent – normal jet; ●, turbulent – with microjets.

the dynamics of the large-scale structures is central and is described as superposition of instability waves. Specifically, Viswanathan & Morris relate the vorticity thickness growth rates to the disturbance amplification rates. As pointed out in a review by Michalke (1984), there are a number of parameters that influence the amplification rates, with frequency being an important one. Another significant variable is the form of the turbulent mean velocity profile; and for theoretical analysis, several have been used. Two common ones, and termed as profile 2 and profile 3 by Michalke, are:

$$\text{Profile 2:} \quad \frac{U}{U_0} = 0.5\left\{1 + \tanh\left[b_2\left(R_{1/2}/r - r/R_{1/2}\right)\right]\right\},$$

where $b_2 = 0.25\, R_{1/2}/\theta$.

$$\text{Profile 3:} \quad \frac{U}{U_0} = \exp\left\{n\left[b_3\left(r/R_{1/2} - 1\right) + 1\right]^2\right\},$$

where $b_3 = 0.312\, R_{1/2}/\theta$ and $n = 0$ for $r/R_{1/2} \leqslant 1 - 1/b_3$, elsewhere $n = -\ln 2$.

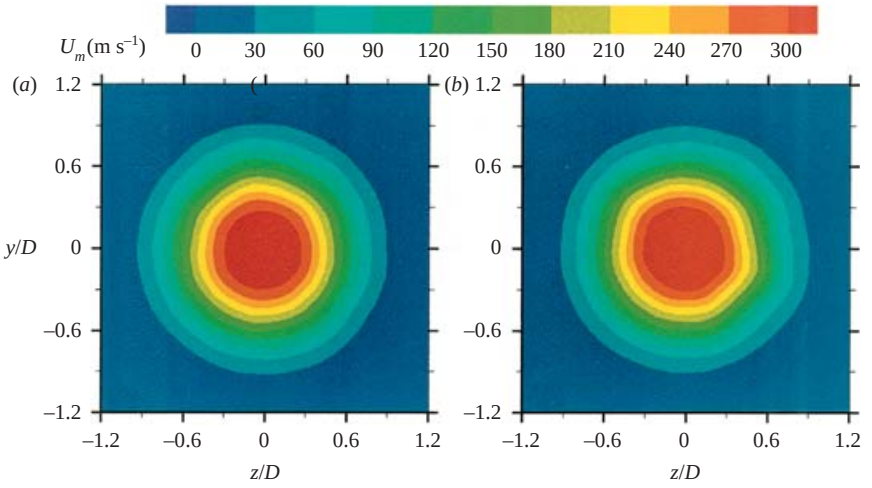

FIGURE 14. Mean velocity distribution in the cross-sectional plane at $x/D = 4$. (*a*) Normal jet; (*b*) with microjets.

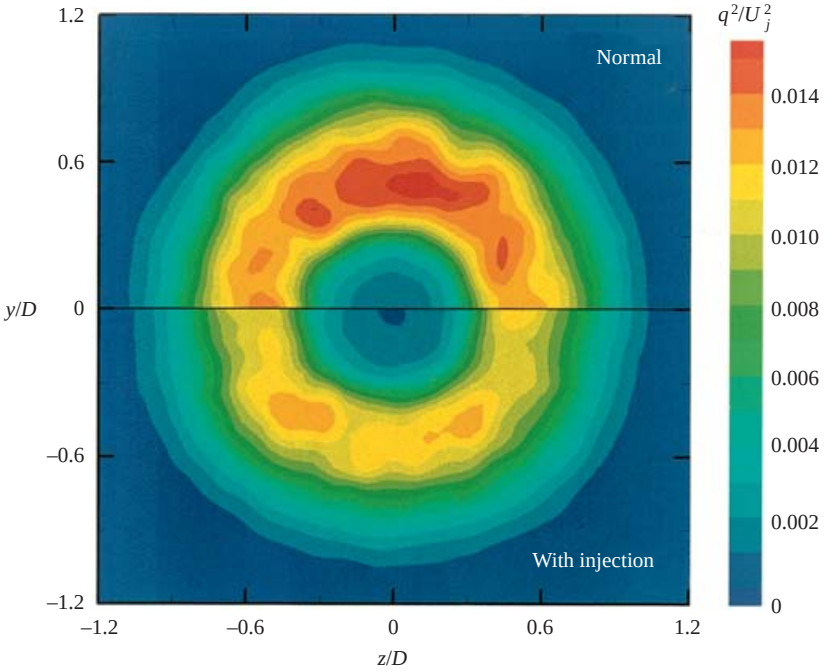

FIGURE 15. Distribution of the total turbulent kinetic energy in the cross-sectional plane at $x/D = 4$. Upper half – normal; lower half – with microjects.

In the above, U_0 is the velocity at $r = 0$, $R_{1/2}$, as indicated earlier, is the radius at which $U/U_0 = 0.5$ and θ is the shear-layer momentum thickness. One of the parameters which certainly characterizes the profile is the ratio $\theta/R_{1/2}$; it is known that the profiles tend to be more stable as the value of the ratio increases. However, as pointed out by Cohen & Wygnasky (1987), profiles having very similar values of

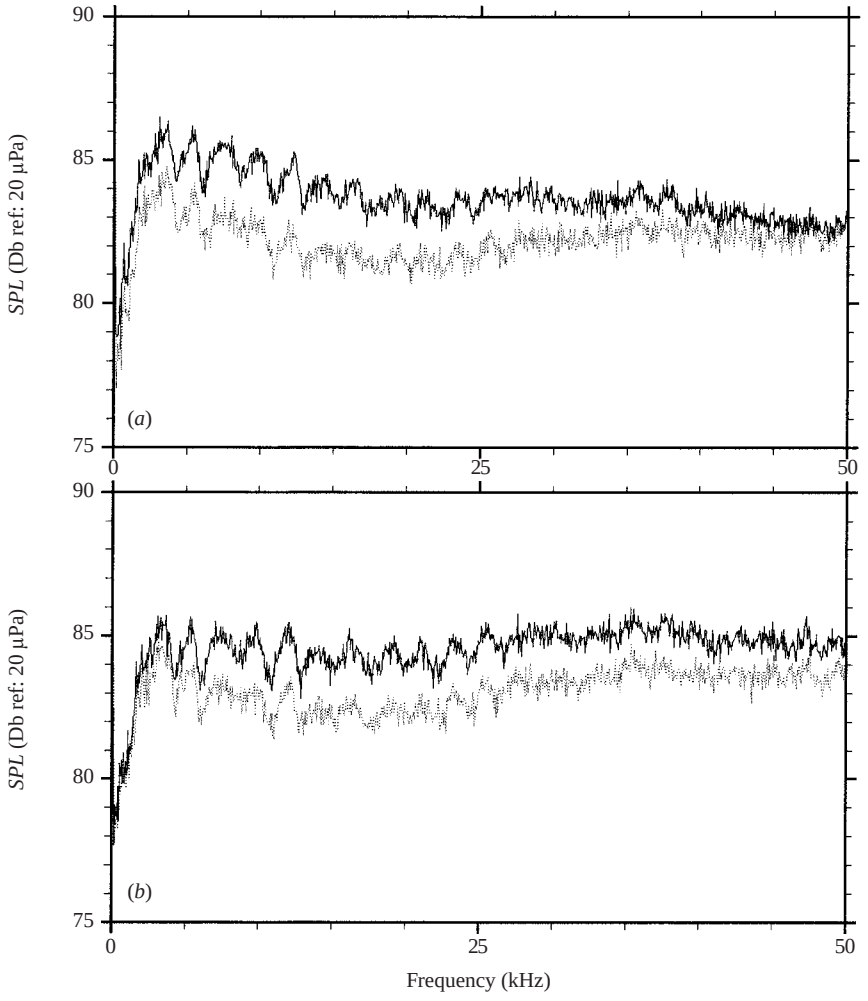

FIGURE 16. Near-field noise spectra at 90° from the jet axis with the exit boundary layer being (*a*) laminar and (*b*) turbulent. ———, normal; · · ·, with microjets.

$\theta/R_{1/2}$ can have differing stability properties if there are other more subtle variations, like the maximum gradient. This observation has also been made by Michalke, who points out that in addition to $\theta/R_{1/2}$, the vorticity distribution characterized by its maximum value could be important. The lower the value of the peak-normalized vorticity, the more stable is the profile.

In figure 17, we present the measured velocity profiles in a suitably normalized form at axial locations of $x/D = 1,\ 2,\ 3$ and 4; the corresponding normalized vorticity distributions are presented in figure 18 (the kinks in these are evidently due to the microjets, when used). The normal measured profiles seem to match very well the analytical profiles 2 and 3 indicated above. However, with the use of microjets, there are significant differences and, in particular, the peak vorticity is reduced, thus making the profiles more stable. In addition, there is an increase in the magnitude of $\theta/R_{1/2}$ for the mean velocity profiles with microjets; however, the change is more marginal than what is observed in the peak vorticity. This is apparent from the plots of $\theta/R_{1/2}$

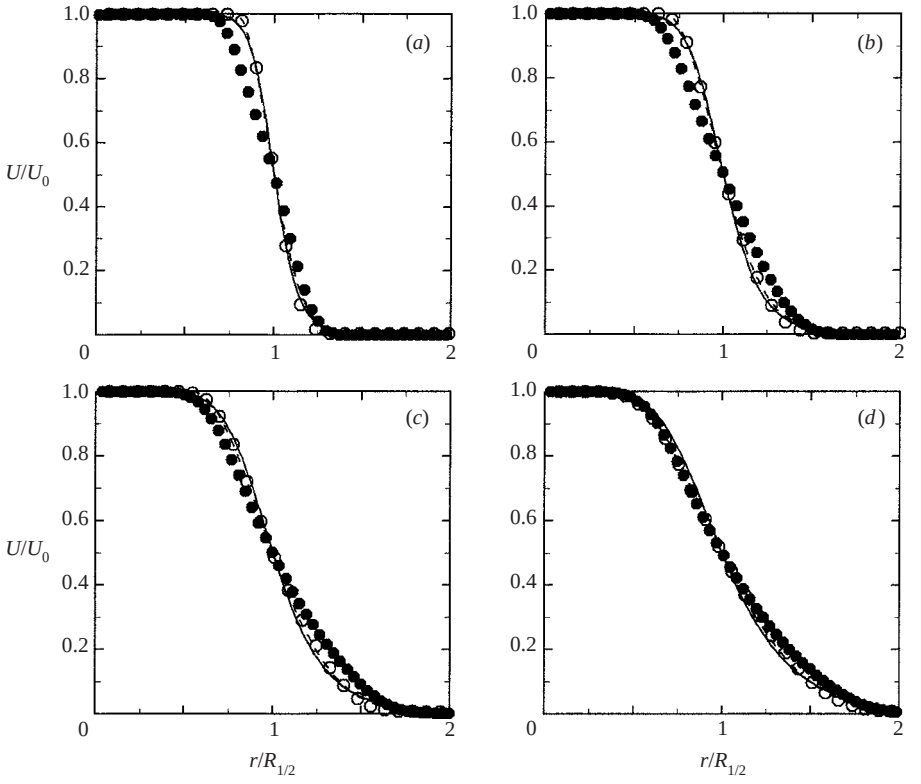

FIGURE 17. Normalized mean velocity profiles. (*a*) $x/D = 1$; (*b*) 2; (*c*) 3; (*d*) 4. ○, normal; ●, with microjets; ———, analytical profile 2; ---, analytical profile 3.

(we also computed $\theta_c/R_{1/2}$, see Michalke (1984) for the definition of θ_c, to include compressible effects; however, the differences between θ and θ_c were too small to be of any concern) and the normalized peak vorticity, $\Omega_{max}R_{1/2}/U_0$, as a function of x/D shown in figures 19 and 20. It should be noted from the results presented in figures 17–20 that the effect of microjets on the mean velocity parameters is limited to an axial distance of about $x/D = 4$; it may not be coincidental that it is in this region in which the maximum reductions in the turbulent intensities are also observed.

The combined effect of an increase in $\theta/R_{1/2}$ and a decrease in $\Omega_{max}R_{1/2}/U_0$ means a substantially more stable jet (Michalke 1984; Cohen & Wygnasky 1987), at least initially, and this fact could be a convincing explanation for the observed effects due to microjets.

The effects can be considered from another point of view, but still within the linear stability framework. The amplification rate, $-\alpha_i$, for a jet without coflow is governed by the relation (Michalke 1984; Morris 1977)

$$-\alpha_i\theta = f(a_r\theta)$$

where α_r is the (real) wavenumber, and θ is the shear-layer momentum thickness. For a given type of velocity profile (tanh, for example), the function f is universal and for parallel-flow analysis the maximum normalized amplification rate is 0.117. Therefore, the actual amplification rate, $-\alpha_i$, clearly reduces with increasing θ. The essence of this argument can be extended to non-parallel flow considerations. Hence, the reason

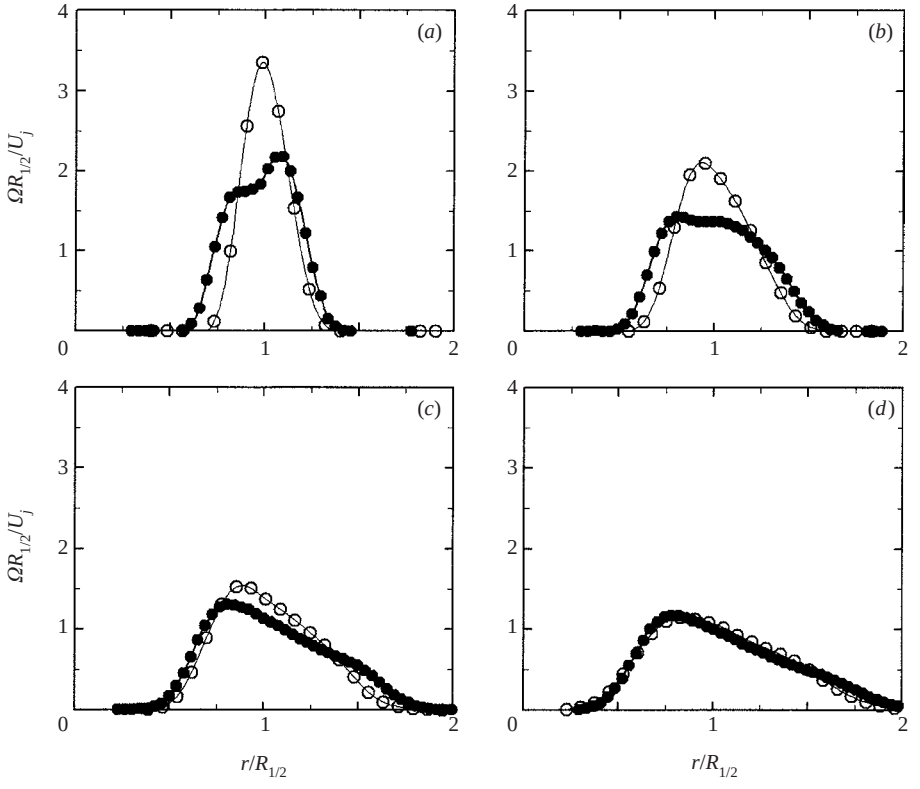

FIGURE 18. Normalized vorticity distribution. (*a*) $x/D = 1$; (*b*) 2; (*c*) 3; (*d*) 4. ○, normal; ●, with microjets.

for stabilization could simply be interpreted in terms of the fact that the microjets produce a larger initial shear-layer thickness. It could also be argued that, if the comparison of the profiles shown in figure 17 were made at the same $(x - x_0)/D$, the profiles would collapse. However, close examination of the modified profiles shows that this will not be the case since the microjets introduce subtle changes in the shape of the velocity profiles. For example, in figure 17(*a*) it should be noted that the effect of microjets is more on the high-speed side than the low-speed side. Thus, the profiles are not symmetric and such effects could influence the stability characteristics. Because of this, the approach of viewing the effect of the microjets in terms of modifications of the velocity profiles would be more appropriate than viewing it in terms of just modification of the initial shear-layer thickness.

Even though, based on the existing evidence, the above explanations for the physical mechanism behind the effects due to microjets seem most plausible, there could be other possibilities. One such is associated with the presence of streamwise vorticity, which is contained in two counter-rotating vortices in a familiar kidney shape once the microjets are bent over by the primary jet (Andreopoulos & Rodi 1984). It is found that injection of streamwise vorticity in a plane shear-layer using added protuberances could influence the structure and growth of a turbulent mixing layer (Bell & Mehta 1993). In particular, both the growth rate and turbulence intensities are measured to be lower in the presence of spanwise perturbations, as compared to those under normal conditions. However, Bell & Mehta found these effects to be present only

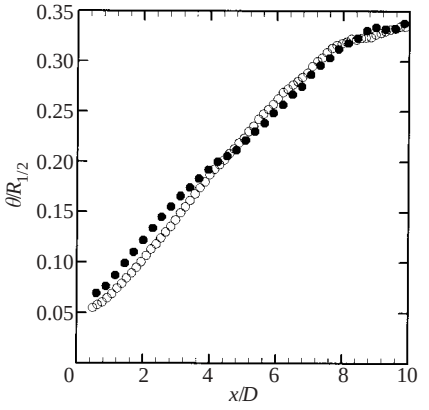

FIGURE 19. Axial variation of normalized momentum thickness. ○, normal; ●, with microjets.

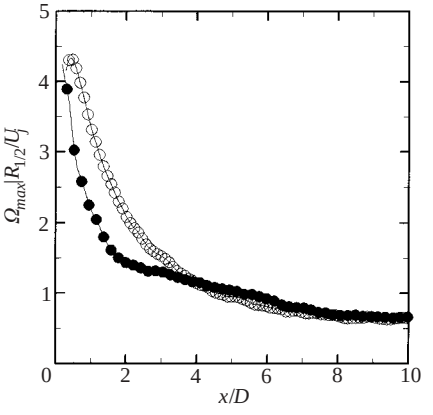

FIGURE 20. Axial variation of peak normalized vorticity. ○, normal; ●, with microjets.

when relatively strong streamwise vortical structures were generated. They also found that, under these conditions, the reduced growth rates persist in the far field; whereas, we do not observe this with the use of microjets. Hence, the question to be addressed is whether the streamwise vortices resulting from the interaction of the microjets with the primary jet flow can be considered strong or weak in relation to the strength of the dominant azimuthal vortex structures. The first indication based on the PIV studies is that they are weak. The possibility that even relatively weak streamwise vortex structures can destroy the azithumal coherence of the large-scale structures and thus reduce their strength, cannot, however, be ruled out.

5. Concluding remarks

The questions raised above and the detailed nature of the aerodynamic interaction of the microjets with the main jet, which result in the observed mean velocity profile changes, can perhaps best be investigated using direct numerical simulations (DNS). In particular, these may help in arriving at the optimum conditions for the

effectiveness of the microjets. Some of the parameters which can be varied are: the angle of injection; the mass flux ratio; the momentum flux ratio; the diameter ratio; the azimuthal spacing ratio; and the physical properties of the microjet gas. In fact, DNS studies have advanced to the extent of predicting radiated noise levels from both high subsonic and supersonic jets (Freund 2001; Freund, Lele & Moin 2000). It would be of great interest to see if such computations can show significant noise suppression owing to the use of microjets under supersonic conditions, when the possibilities for noise radiation by Mach wave emission are favourable.

Financial support from ONR, NASA and Boeing is gratefully acknowledged.

REFERENCES

Alkislar, M. B. 2001 Flow field measurements in a screeching rectangular jet. PhD thesis, Dept Mechanical Engineering, Florida State University.

Alvi, F. S., Elavarasan, R., Shih, C., Garg, G. & Krothapalli, A. 2000 Active control of supersonic impinging jets using microjets. *AIAA Paper* 2000-2236.

Alvi, F. S., Krothapalli, A., Washington, D. & King, C. J. 1996 Aeroacoustic properties of a supersonic diamond-shaped jet. *AIAA J.* **34**, 1562–1569.

Anderson, B., Wygnaski, I. & Gutmark, E. 1999 Noise reduction by interaction of flexible filaments with an underexpanded supersonic jet. *AIAA Paper* 99-0080.

Andreopoulos, J. & Rodi, W. 1984 Experimental investigation of jets in a crossflow. *J. Fluid Mech.* **138**, 93–127.

Batchelor, G. K. & Gill, A. E. 1962 Analysis of the stability of axisymmetric jets. *J. Fluid Mech.* **14**, 529–551.

Bell, J. H. & Mehta, R. D. 1993 Effects of imposed spanwise pertubations on plane mixing-layer structure. *J. Fluid Mech.* **257**, 33–63.

Bernal, L. P. & Roshko, A. 1986 Streamwise vortex structure in plane mixing layers. *J. Fluid Mech.* **170**, 499–525.

Bishop, K. A., Ffowcs Williams, J. F. & Smith, W. 1971 On the noise of the unsuppressed high-speed jet. *J. Fluid Mech.* **50**, 21–31.

Bradshaw, P., Ferriss, D. H. & Johnson, R. F. 1964 Turbulence in the noise-producing region of a circular jet. *J. Fluid Mech.* **19**, 591–625.

Bradshaw, P. 1966 The effect of initial conditions on the development of a free shear layer. *J. Fluid Mech.* **26**, 225–236.

Chan, Y. Y. 1977 Wavelike eddies in a turbulent jet. *AIAA J.* **15**, 992–1001.

Cohen, J. & Wygnasky, I. 1987 The evolution of instabilities in the axisymmetric jet. Part 1. The linear growth of disturbances near the nozzle. *J. Fluid Mech.* **176**, 191–219.

Crighton, D. G. 1981 Acoustics as a branch of fluid mechanics. *J. Fluid Mech.* **106**, 261–298.

Crow, S. C. & Champagne, S. H. 1971 Orderly structure in jet turbulence. *J. Fluid Mech.* **48**, 547–591.

Fisher, M. J., Harper-Bourne, M. & Glegg, S. A. L. 1977 Jet engine noise source location: the polar correlation technique. *J. Sound Vib.* **51**, 23–54.

Freund, J. B. 2001 Noise sources in a low-Reynolds-number turbulent jet at Mach 0.9. *J. Fluid Mech.* **438**, 277–305.

Freund, J. B., Lele, S. K. & Moin, P. 2000 Numerical simulation of a Mach 1.92 turbulent jet and its sound field. *AIAA J.* **38**, 2023–2031.

Hussain, A. K. M. F. 1983 Coherent structures – reality and myth. *Phys. Fluids* **26**, 2816–2850.

Hussain, A. K. M. F. & Zedan, M. F. 1978 Effects of the initial condition on the axisymmetric free shear layer: effects of the initial momentum thickness. *Phys. Fluids* **21**, 1100–1112.

Jiminez, J. 1983 A spanwise structure in the plane shear layer. *J. Fluid Mech.* **132**, 319–336.

Kibens, V. 1980 Discrete noise spectrum generated by an acoustically excited jet. *AIAA J.* **18**, 434–441.

Krothapalli, A., Rajkuperan, E., Alvi, F. & Lourenco, L. 1999 Flow field and noise characteristics of a supersonic impinging jet. *J. Fluid Mech.* **392**, 155–181.

Lau, J. C., Morris, P. J. & Fisher, M. J. 1979 Measurements in subsonic and supersonic free jets using a laser velocimeter. *J. Fluid Mech.* **93**, 1–27.

Laufer, J., Schlinker, R. & Kaplan, R. E. 1976 Experiments on supersonic jet noise. *AIAA J.* **14**, 489–497.

Lepicovsky, K. K., Ahuja, K. K., Brown, W. H. & Burrin, R. H. 1987 Coherent large-scale structures in high Reynolds number supersonic jets. *AIAA J.* **11**, 1419–1425.

Liepmann, D. & Gharib, M. 1992 The role of streamwise vorticity in the near-field entrainment of round jets. *J. Fluid Mech.* **245**, 643–668.

Liu, J. T. C. 1974 Developing large scale wavelike eddies and the near field jet noise. *J. Fluid Mech.* **62**, 437–464.

Lourenco, L. M. & Krothapalli, A. 1998 Mesh-free second order accurate algorithm for PIV processing. *Proc. Intl Conf. on Optical Technology and Image Processing in Fluid, Thermal and Combustion Flows, Yokohama, Japan, December 1998*, p. 224.

McCormick, D. C. & Bennett, J. C. 1993 Vortical and turbulent structure of a lobed mixer free-shear layer. *AIAA Paper* 93-0219.

Michalke, A. 1971 Instabilitat eines kompressiblen runden freistrahls unter berucksichtigung des einflusses der strahlgrenzschichtdicke. *Z. Flugwiss.* **19**, 319–328. (English translation *NASA TM* 75190, 1977).

Michalke, A. 1984 Survey on jet instability theory. *Prog. Aerospace Sci.* **21**, 159–199.

Mollo-Christensen, E. 1967 Jet noise and shear flow stability seen from an experimenter's viewpoint. *J. Appl. Mech.* E **89**, 1–10.

Moore, C. J. 1977 The role of shear-layer instability waves in jet exhaust noise. *J. Fluid Mech.* **80**, 321–367.

Morris, P. J. 1976 Turbulence measurements in subsonic and supersonic axisymmetric jets in a parallel stream. *AIAA J.* **14**, 1468–1475.

Morris, P. J. 1977 The spatial viscous instability of axisymmetric jets. *J. Fluid Mech.* **77**, 511–529.

Morris, P. J., Giridharan, M. G. & Lilley, G. M. 1990 On the turbulent mixing of compressible free shear layers. *Proc. R. Soc. Lond.* A **431**, 219–243.

Narayanan, S., Barber, T. J. & Polak, D. R. 2002 High subsonic jet experiments: turbulence and noise generation studies. *AIAA J.* **40**, 430–437.

Norum, T. D. & Seiner, J. M. 1982 Broadband shock noise from supersonic jets. *AIAA J.* **20**, 68–73.

Oertel, H. 1979 Mach wave radiation of hot supersonic jets. In *Mechanics of Sound Generation in Flows* (ed. E. A. Mueller), pp. 275–281. Springer.

Phillips, O. M. 1960 On the generation of sound by supersonic turbulent shear layers. *J. Fluid Mech.* **9**, 1–28.

Powell, A. 1953 On the mechanism of choked jet noise. *Proc. Phys. Soc. Lond.* B **66**, 1039–1057.

Schaffer, M. 1979 Direct measurements of the correlation between axial in-jet velocity fluctuations and far field noise near the axis of a cold jet. *J. Sound Vib.* **64**, 73–83.

Siddavaram, V. 2002 Flow characterization of a Mach 0.9 axisymmetric jet using particle image velocimetry. MS thesis, Dept Mechanical Engineering, Florida State University.

Simonich, J. C., Narayanan, S., Barber, T. J. & Nishimura, M. 2001 Aeroacoustic characterization, noise reduction, and dimensional scaling effects of high subsonic jets. *AIAA J.* **39**, 2062–2069.

Stromberg, J. L., McLaughlin, D. K. & Troutt, T. R. 1980 Flow field and acoustic properties of a Mach number 0.9 jet at a low Reynolds number. *J. Sound Vib.* **72**, 159–176.

Tam, C. K. W. & Burton, D. E. 1984 Sound generated by instability waves of supersonic flows. Part 2. Axisymmetric jets. *J. Fluid Mech.* **138**, 273–295.

Tam, C. K. W. & Hu, F. Q. 1989 On the three families of instability waves of high-speed jets. *J. Fluid. Mech.* **201**, 447–483.

Troutt, T. R. & McLaughlin, D. K. 1982 Experiments on the flow and acoustic properties of a moderate Reynolds number supersonic jet. *J. Fluid Mech.* **116**, 123–156.

Viswanathan, K. & Morris, P. J. 1992 Predictions of turbulent mixing in axisymmetric compressible shear layers. *AIAA J.* **30**, 1529–1536.

Yule, A. J. 1978 Large-scale structure in the mixing layer of a round jet. *J. Fluid Mech.* **89**, 413–432.

Zaman, K. B. M. Q. 1994 Effects of delta tabs on mixing and axis switching in jets from axisymmetric nozzles. *AIAA Paper* 94-0186.

Zaman, K. B. M. Q. 1999 Spreading characteristics of compressible jets from nozzles of various geometries. *J. Fluid Mech.* **383**, 197–228.

Zaman, K. B. M. Q. & Hussain, A. K. M. F. 1984 Natural large-scale structures in the axisymmetric mixing layer. *J. Fluid Mech.* **138**, 325–351.